



Grubbs-Hoveyda catalysts conjugated to a β -barrel protein: Effect of halide substitution on aqueous olefin metathesis activity

Aaron A. Ingram^{a,1}, Dong Wang^{a,b}, Ulrich Schwaneberg^b, Jun Okuda^{a,*}

^a Institute of Inorganic Chemistry, RWTH Aachen University, Landoltweg 1, 52074 Aachen, Germany

^b Institute of Biotechnology, RWTH Aachen University, Worringerweg 3, 52074 Aachen, Germany

ARTICLE INFO

Keywords:

Olefin metathesis
Artificial metalloenzymes
Biohybrid catalysts
 β -Barrel protein
Ruthenium

ABSTRACT

The effect of halide substitution in Grubbs-Hoveyda II catalysts (GHII catalysts) embedded in the engineered β -barrel protein nitrobindin (NB4exp) on metathesis activity in aqueous media was studied. Maleimide tagged dibromido and diiodido derivatives of the GHII catalyst were synthesized and covalently conjugated to NB4exp. The biohybrid catalysts were characterized spectroscopically confirming the structural integrity. When the two chloride substituents at ruthenium center were exchanged against bromide and iodide, the diiodo derivative was found to show significantly higher catalytic activity in ring-closing metathesis of α,ω -diolefins, whereas the dibromido derivative was less efficient when compared with the parent dichlorido catalyst. Using the diiodido catalyst, high turnover numbers of up to 75 were observed for ring-closing metathesis (RCM) yielding unsaturated six- and seven-membered N-heterocycles.

1. Introduction

With no equivalent in nature, olefin metathesis represents an attractive biorthogonal reaction that offers a wide application scope for C=C bond cleavage and forming catalysis in biological systems. [1–4] Ruthenium-catalyzed olefin metathesis is predestinated for these reactions as the catalysts display a high tolerance towards water and air. [5,6] Examples include application in chemo-enzymatic cascade reactions, [7–11] chemical modification of biomolecules, [12–15] use as biosensors, [16,17] olefin metathesis in living cells [18,19] and in vivo drug synthesis. [20–22] While the reaction mechanism and degradation pathways of ruthenium carbene catalysts are well-understood in organic media, mechanistic understanding of olefin metathesis in water is still limited. [3] Aqueous olefin metathesis can be optimized by performing the reaction in acidic media [23] and by adding chloride salts to the solution. [24] This prevents the halide-exchange leading to dihydroxy complexes and binuclear species [25] as the major decomposition pathway in water (Fig. 1). [26] A recent report demonstrates that the exchange of the chloride ligand with a nitrate group improved the activity of a water-soluble second generation Grubbs-Hoveyda catalyst

(GHII catalyst) in the presence of biological additives such as phosphate buffer and glutathione. [27] This suggests that the halide ligand might be a key for improving the efficiency of aqueous olefin metathesis.

Another recent approach for optimizing aqueous olefin metathesis is the development of artificial metalloenzymes as biohybrid catalysts, [20,28–35] which consist of artificial metal-based cofactors conjugated to a protein. [36] Biohybrid catalysts can be utilized to carry out biorthogonal reactions in biological environments [37] but can also be used to combine mutually incompatible reactions. [10,11] Tanaka et al. developed a biohybrid catalyst based on an iodide-substituted GHII catalyst which is stable against decomposition in aqueous media when compared to the dichloride parent. [22] Halide substituted GHII catalysts played rather a niche role, [38–51] but recent reports describe their higher stability against air [50] and water compared to the chloride parent species. [52,53] Effects of the metal first coordination sphere in biohybrid catalysts has only been investigated to a limited extent. [54] Here, we report biohybrid catalysts based on halide substituted GHII catalysts conjugated to an engineered variant of the β -barrel protein nitrobindin NB4exp. [55] NB4exp proved to be a robust scaffold for biohybrid catalysts promoting to different types of olefin metathesis

Abbreviations: CD, Circular dichroism; ESI MS, Electrospray Ionization Mass Spectrometry; GHII catalyst, second generation Grubbs-Hoveyda catalyst; NHC, N-Heterocyclic Carbene; ICP-OES, Inductively Coupled Plasma – Optical Emission Spectrometry; NB4exp, Engineered variant of *Arabidopsis thaliana* nitrobindin with two duplicated β -strands; NMR, Nuclear Magnetic Resonance; RCM, Ring-closing Metathesis; TON, Turnover Number.

* Corresponding author.

E-mail address: jun.okuda@ac.rwth-aachen.de (J. Okuda).

¹ Current address: Department of Biotechnology, Delft University of Technology, Van der Maasweg 9, 2629 HZ Delft, The Netherlands

<https://doi.org/10.1016/j.jinorgbio.2024.112616>

Received 30 March 2024; Received in revised form 15 May 2024; Accepted 18 May 2024

Available online 24 May 2024

0162-0134/© 2024 The Authors. Published by Elsevier Inc. This is an open access article under the CC BY-NC license (<http://creativecommons.org/licenses/by-nc/4.0/>).

(cross-metathesis, RCM and ring-opening metathesis polymerization) [55,56] and numerous other reactivities. [57–67] A goal of this work was to understand the effect of the halide-substitution in Grubbs-Hoveyda catalyst on the olefin metathesis reactivity in different reaction media.

2. Experimental section

2.1. General information

All experiments were performed under a nitrogen or argon atmosphere using standard Schlenk techniques or an MBraun argon or nitrogen-filled glovebox. Chemicals were purchased from Merck, TCI and other common suppliers. Acetone was dried over activated molecular sieves. DMSO and 1,4-dioxane were degassed by using “pump-freeze-thaw” cycles. Water was degassed by bubbling with argon for at least one hour. The maleimide tagged GH-catalyst (**Ru-Cl₂**) was prepared according to previously reported procedures. [34] RCM substrates and products were synthesized according to previously reported procedures.

The pH values were measured with Voltcraft KBM-110 pH-meter Redox. NMR spectra were recorded on a Bruker Avance III HD 400 NMR spectrometer. Chemical shifts are reported in ppm relative to residual solvent resonances. [68] ESI-MS analysis was performed on a Thermo Fisher Scientific LTQ Orbitrap XL mass spectrometer. Circular dichroism (CD) spectra were recorded on a JASCO J1100 CD spectrometer. UV/VIS spectra were recorded on a JASCO J1100 CD spectrometer (for proteins). IR spectra were recorded on a Shimadzu IRSpirit spectrometer fitted with a Single Reflection ATR accessory. ICP-OES measurements were conducted on a Spectro Analytical Instruments Spectroblue ICP-OES spectrometer. Gas chromatography (GC-MS) was performed on a Shimadzu GCMS-QP2010 Plus equipped with a Macherey Nagel FS-Surpreme-5 ms PLUS column (30 m × 0.25 mm, 0.5 μm) with helium as carrier gas. The gradient was carried out as follows: Injector temperature 340 °C; 120 °C for 2 min, ramp with 10 °C min⁻¹ to 300 °C, 2 min at 300 °C.

2.2. Synthesis of halide-substituted GH-catalysts

2.2.1. Synthesis of Ru-Br₂

Ru-Cl₂ (52 mg, 65 μmol, 1.0 equiv.) was dissolved in acetone (20 mL) and sodium bromide (3.72 g, 36.1 mmol, 560 equiv.) was added. The reaction solution was stirred at room temperature for 72 h. The solid was removed by filtration. The filtrate was concentrated under reduced pressure and repeatedly taken up in toluene. Remaining precipitate was removed by filtration and the product was obtained by removing the solvent under reduced pressure. **Ru-Br₂** was obtained as green microcrystals. **Yield:** 56 mg, 62 μmol, 95%. ¹H NMR (CD₂Cl₂, 400 MHz): δ [ppm] = 16.46–16.20 (m, 1H, Ru=CH), 7.60 (td, *J* = 7.9, 1.7 Hz, 1H, Ar-H), 7.17–6.95 (m, 5H, Ar-H), 6.96–6.83 (m, 2H, Ar-H), 6.66 (s, 2H, C=CH), 5.05–4.85 (m, 1H, C(CH₃)₂CH), 4.77–4.54 (m, 1H, N-CH-CH₂), 4.32 (t, *J* = 11.0 Hz, 1H, N-CH₂-CH), 4.28–4.10 (m, 2H, N-CH-CH₂O), 4.00 (dd, *J* = 10.8, 7.1 Hz, 1H, N-CH₂-CH), 3.51 (t, *J* = 6.9 Hz, 2H, N-CH₂-CH₂), 2.82–2.20 (m, 20H, Ar-CH₃ / CO-CH₂-), 1.85 (p, *J* = 7.1 Hz,

2H, CO-CH₂-CH₂), 1.45–1.22 (m, 6H, C(CH₃)₂CH). ¹³C NMR (CD₂Cl₂, 100 MHz): δ [ppm] = 299.5 (br), 215.7 (br), 173.0, 171.3, 152.8, 146.0, 140.9, 140.3, 134.0, 138.8, 138.6, 138.0, 134.8, 134.6, 130.6, 130.5, 130.2, 130.0, 129.7, 129.5, 128.7, 125.8, 122.9, 122.7, 113.8, 76.0, 64.7, 64.1, 63.2, 62.4, 55.8, 54.5, 37.4, 34.7, 31.5, 29.6, 24.1, 22.9, 22.6, 21.9, 21.4, 21.3, 19.3, 14.4. IR (neat): $\tilde{\nu}$ [cm⁻¹] = 2963, 2917, 2862, 2361, 2342, 1736, 1703, 1607, 1588, 1575, 1474, 1452, 1442, 1405, 1259, 1240, 1170, 1139, 1112, 1095, 1033, 1014, 979, 933, 877, 851, 826, 804, 745, 694, 668. ESI HRMS: *m/z* = [M-Br]⁺ calc. 832.1743, observed 832.1722.

2.2.2. Synthesis of Ru-I₂

Ru-Cl₂ (100 mg, 122 μmol, 1.0 equiv.) and sodium iodide (10.0 g, 66.7 mmol, 550 equiv.) were dissolved in acetone (10 mL). The reaction mixture was stirred at room temperature for 36 h. Toluene (50 mL) was added to precipitate excess sodium iodide. Acetone was removed under reduced pressure and the precipitate was removed by filtration. The filtrate was concentrated under reduced pressure and repeatedly taken up in toluene. Remaining precipitate was removed by filtration and the product was obtained by removing the solvent under reduced pressure. **Ru-I₂** was obtained as dark green microcrystals. **Yield:** 102 mg, 101 μmol, 83%. ¹H NMR (CD₂Cl₂, 400 MHz): δ [ppm] = 15.65 (s, 0.7H, Ru=CH), 15.60 (s, 0.3H, Ru=CH), 7.64 (ddd, *J* = 8.8, 7.3, 1.8 Hz, 1H, Ar-H), 7.33–6.99 (m, 5H, Ar-H), 6.98–6.88 (m, 2H, Ar-H), 6.70 (d, *J* = 4.5 Hz, 2H, C=CH), 5.17–4.95 (m, 0.7H, C(CH₃)₂CH), 4.78–4.64 (m, 0.3H, C(CH₃)₂CH), 4.65–4.48 (m, 1H, N-CH-CH₂), 4.42–4.14 (m, 3H, N-CH₂-CH / N-CH-CH₂O), 4.04 (dd, *J* = 10.7, 6.0 Hz, 1H, N-CH₂-CH), 3.56 (td, *J* = 6.9, 3.8 Hz, 2H, N-CH₂-CH₂), 2.86 (s, 2H, Ar-CH₃), 2.71 (s, 1H, Ar-CH₃), 2.63–2.43 (m, 12H, Ar-CH₃), 2.43–2.31 (m, 5H, Ar-CH₃ / CO-CH₂-), 1.99–1.81 (m, 2H, CO-CH₂-CH₂), 1.54 (dd, *J* = 22.4, 6.1 Hz, 5H, C(CH₃)₂CH), 1.41 (dd, *J* = 8.5, 6.1 Hz, 1H, C(CH₃)₂CH). ¹³C NMR (CD₂Cl₂, 101 MHz): δ [ppm] = 299.4, 299.2, 298.3, 298.1, 217.4, 216.9, 173.1, 172.8, 171.3, 153.5, 153.4, 145.7, 145.4, 140.0, 139.8, 139.5, 138.6, 138.4, 137.8, 137.6, 136.9, 136.1, 134.6, 134.3, 131.2, 131.1, 131.0, 130.7, 130.4, 130.1, 130.0, 130.0, 129.5, 128.7, 125.8, 123.3, 122.4, 114.0, 76.6, 76.4, 64.6, 64.0, 63.6, 62.7, 55.9, 37.4, 31.7, 31.6, 29.7, 24.3, 24.1, 23.9, 23.0, 22.4, 22.3, 22.1, 22.0, 21.4, 21.3, 20.9, 20.5. IR (neat): $\tilde{\nu}$ [cm⁻¹] = 2959, 2916, 2857, 2359, 2341, 1736, 1704, 1605, 1590, 1575, 1474, 1451, 1441, 1406, 1374, 1259, 1238, 1220, 1169, 1137, 1112, 1095, 1033, 1014, 977, 931, 877, 850, 838, 824, 745, 695, 668. ESI HRMS: *m/z* = [M-I]⁺ calc. 876.1446, observed 876.1446.

2.3. Preparation of the biohybrid catalysts

NB4exp was prepared as previously described. [55] A preculture of 5.0 mL of LB-medium (supplemented with 50 μg mL⁻¹ of kanamycin) was inoculated with *E. coli* BL21 Gold (DE3) harboring a pET42(+) vector containing a gene encoding NB4exp fused N-terminally with a Strep-tag and incubated at 37 °C with 250 rpm shaking for 17 h. A main culture of 200 mL TB-medium (supplemented with 50 μg mL⁻¹ kanamycin) was inoculated with 1.0 mL of the preculture and incubated at 37 °C with 250 rpm shaking until an OD₆₀₀ of 0.6–0.8 was reached. Protein expression was induced by addition of 0.5 mM of IPTG and the

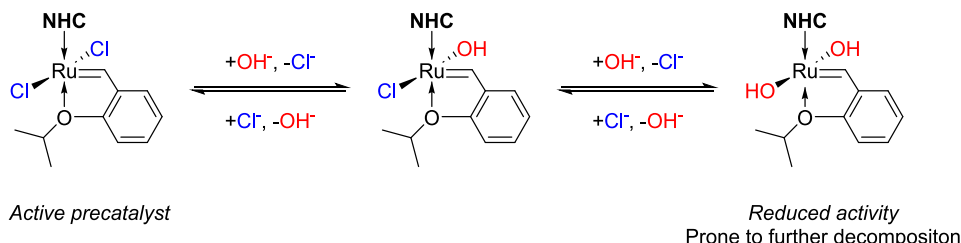


Fig. 1. Degradation of GHII catalysts in aqueous environments by ligand exchange of chloride with hydroxide.

temperature was set to 18 °C for 20 h. Cells were harvested by centrifugation (4000 xg, 20 min, 4 °C) and washed with 50 mM of potassium phosphate buffer (pH 7.0). The cells were suspended with 20 mM of Tris-HCl (pH 8.0) containing 300 mM of sodium chloride (1:8 *m,v*) and disrupted by sonification on using a sonotrode. The cell debris and insoluble protein fraction was removed by centrifugation (15,000 xg, 45 min, 4 °C). The supernatant was filtered through a syringe filter (0.45 µm pore size) and loaded onto a StrepTactin Sepharose column and washed with 10 cv of 20 mM Tris-HCl (pH 7.0) containing 300 mM of sodium chloride. NB4exp was eluted by 1 mM of desthiobiotin in the same buffer. The fractions contained the desired protein were pooled and subjected to a buffer change towards potassium phosphate buffer (50 mM, pH 7.0) using a HiTrap Desalting column (5 mL bed volume). Purified protein was stored shortly (<3 h) at 4 °C until further use. Alternatively, the protein can be stored at -45 °C when frozen in liquid nitrogen prior to storage.

In a glovebox under N₂-atmosphere, protein (20 µM) in Tris-buffer (10 mM, pH 7.4) containing 250 mM of potassium halide salt and 10 vol% DMSO was incubated with catalysts **Ru-X₂** (100 µM, 5.0 equiv.) one hour. The solution was shortly centrifuged (10 min, 12,000 x g), the supernatant was concentrated to <1.0 mL using an Amicon centrifugal filter (cutoff Mw 10,000) and subjected to size exclusion chromatography using a HiTrap Desalting column (5 mL bed volume). Protein was eluted using 200 mM potassium halide salt for use in catalytic reactions or potassium phosphate buffer (50 mM, pH 7.0) for analytical purposes. The protein concentration was determined by BCA-assay (Thermo Scientific) according to the manufactures protocol or on a Nanodrop using the calculated molecular weight and absorption at 280 nm.

2.4. Cysteine titration with ThioGlo-1

To 150 µL of a solution of apoprotein or protein conjugated with **Ru-X₂** (5.0 µM) in 50 mM potassium phosphate buffer (pH 7.0), 1.5 µL of a solution of ThioGlo-1 in acetonitrile (1.5 mM; final concentration: 15 µM) was added. The reaction mixture was incubated at room temperature for 30 min and the fluorescence (excitation wavelength 379 nm) at 513 nm was measured. In addition, blank measurements in the absence of protein were performed. All measurements were performed in triplicates.

2.5. Catalytic ring-closing metathesis

The final reaction mixture consisted of 20 mM of buffer (pH 4.0 or 5.5; sodium acetate, sodium citrate, potassium phosphate, MES or pyridine) or alternatively no buffer, 250 mM of potassium halide salt, 30 vol % of dioxane, and 25 µM of **Ru-X₂**@NB4exp in doubly distilled water. The conjugates were diluted from a stock solution of protein in 200 mM of KX solution. The reaction was started by addition of 2.5 mM of the substrate *N,N*-diallyltosylamide from an appropriate stock solution (25 mM in 1,4-dioxane). Reactions were carried out in triplicates at 30 °C with orbital shaking at 900 rpm for 20 h. The reaction was stopped by addition of 375 µL of dichloromethane containing 1.0 mM *n*-tetradecane as internal standard and 6.7 vol% of ethyl vinyl ether. The phases were separated, the organic phase was dried over anhydrous magnesium sulfate and analyzed by GC-MS. Alternatively, reactions were carried out with *N*-allyl-*N*-(3-butenyl)tosylamide or *N*-allyl-*N*-(4-pentenyl)tosylamide instead of *N,N*-diallyltosylamide.

2.6. Molecular modelling

Modelling of the apo-form of NB4exp was performed as reported previously [55,57,58] using YASARA [69] Structure Vers. 20.12.24, employing force field AMBER14. [70] The modelling of the biohybrid catalysts was carried out using GAFF [71] using AM1/BCC [72] partial charges for the catalyst covalently bound to Cys96. [57,58] The metal was replaced by iron since no parameters are available for ruthenium.

To maintain the correct coordination geometry, the distances, and angles from the metal to all coordinating atoms were constrained according to the X-ray structure of the GHII catalysts (Cl, I and with estimated values for Br) by force field arrows. The charge of the metal was set to +2 and the total charge of the catalyst was set to zero. The linker was placed manually in the cavity adjacent to Cys96. A bond from the Cys96 sulfur atom to the C1 atom of the maleimide group was defined, according to the linker geometry in the high-resolution X-ray structure of the rhodium complex. The constructed hybrid catalysts were solvated in a box of TIP3P water molecules using periodic boundaries at pH 7.0 and a density of 0.997 g/mL. Three starting structures were analyzed, and favorable models were identified for covalent attachment to the reactive maleimide atoms by steepest descent minimization and simulated annealing. The pre-minimized structures were relaxed using molecular dynamics calculations at 298 K for 5000 ps and snapshots were taken every 25 ps to analyze the binding modes. Van der Waals volume of the ligand was calculated using Yasara and the MSMS program. [73]

3. Results

3.1. Preparation and characterization of biohybrid catalysts

Halide-substituted homologs of the maleimide tagged **Ru-Cl₂** were prepared by salt metathesis in acetone with a large excess of sodium halide salt to give the complexes in yields of 95% (**Ru-Br₂**) and 83% (**Ru-I₂**). The formation of the disubstituted species was confirmed by ¹H NMR spectroscopy (Figs. S1-S2). In view of different cavity sizes of NB variants (Table S2), we focused on the NB4exp scaffold to ensure accommodation of the heavier halide-substituted complexes. These complexes were covalently conjugated to the Cys96 residue of NB4exp via Michael addition reaction in Tris-HX buffer (10 mM, pH 7.4, 200 mM KX) in the presence of 10% DMSO (Fig. 2a). These conditions ensure the presence of an excess of the corresponding halide salt to prevent ligand exchange with chloride typically contained in biological buffers.

The structure of the biohybrid catalysts was calculated using YASARA structure based on previous molecular modelling [55] and showed similar binding motifs of the complexes in the cavity (Fig. 2b, c, d). No specific interactions between the halide ligands and the protein scaffold were identified. High conjugation efficiencies >95% of the ruthenium complex were determined by ICP-OES measurements (see Table S2). To exclude non-specific interactions between the protein and the metal complex, we further confirmed the conjugation yields by cysteine titration with the maleimide-containing fluorescence dye ThioGlo-1 (Fig. S12). While a solution of free NB4exp showed a significantly increased fluorescence after addition of ThioGlo-1, the samples of **Ru-X₂**@NB4exp exhibited <5% fluorescence, indicating a coupling efficiency of >95%. The biohybrid catalysts obtained were further characterized by ESI MS analysis (Table S3, Figs. S8–11 in the Supporting Information). The calculated mass for catalysts **Ru-Br₂**@NB4exp (*m/z* = 23,427) and **Ru-I₂**@NB4exp (*m/z* = 23,494) was observed in the ESI MS spectra. We further confirmed the structural integrity of NB4exp by CD-spectroscopy (Fig. 3a). The β-barrel of NB4exp has a typical CD-minimum at λ = 217 nm and a maximum below λ = 200 nm. [55] The measured spectra of both the apoprotein and the conjugates match these characteristics well. Thus, the structural integrity of the protein scaffold was confirmed. The prepared biohybrid catalysts were also characterized by UV-Vis spectroscopy (Fig. 3b). The characteristic absorptions bands corresponding to the ligand to metal charge transfer (X→Ru) of the complexes **Ru-Cl₂** (ca. 380 nm), **Ru-Br₂** (ca. 395 nm) and **Ru-I₂** (ca. 415 nm) remain visible after conjugation to NB4exp.

3.2. Ring-closing metathesis of *N,N*-diallyltosylamide as benchmark substrate

Next, we tested our newly prepared biohybrid catalysts (**Ru-**

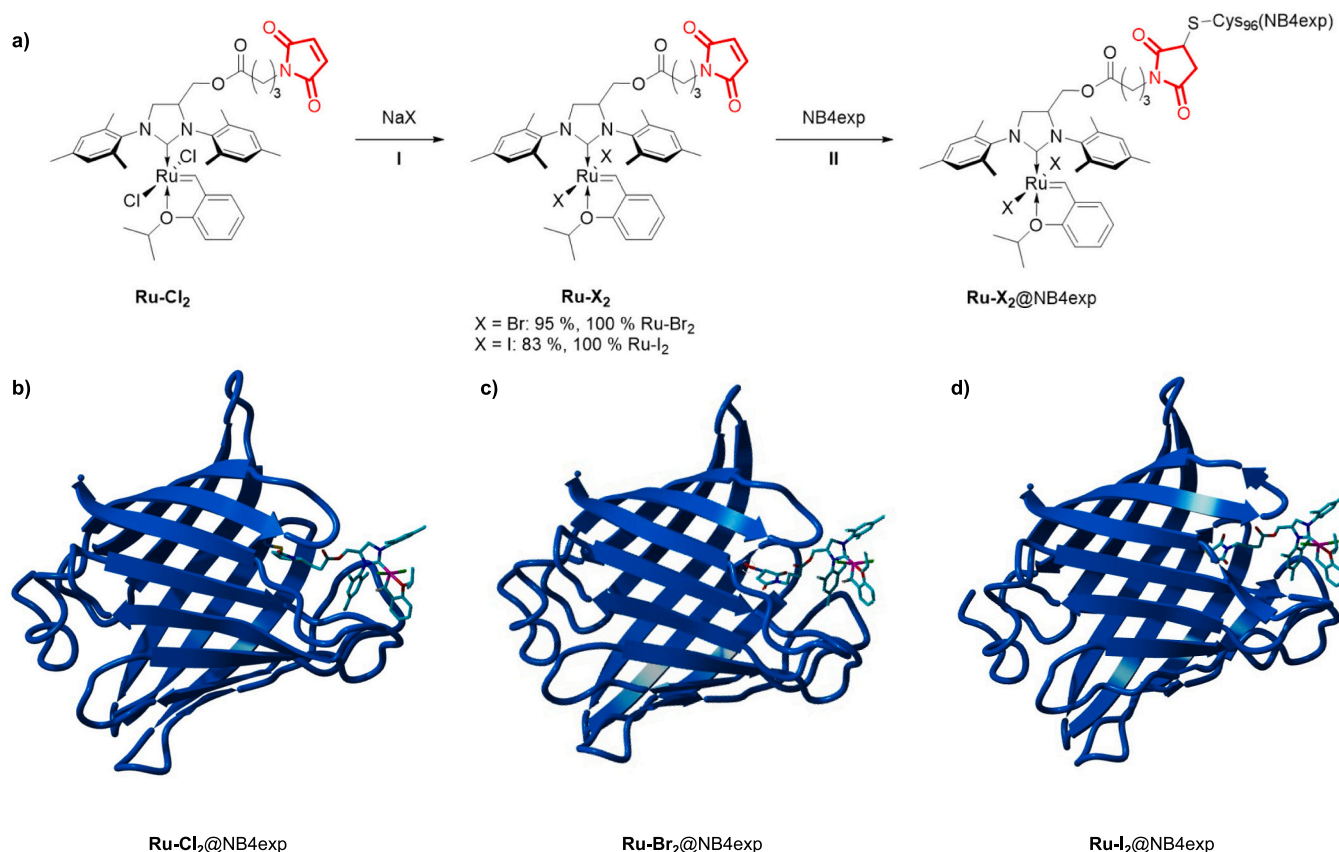


Fig. 2. Preparation and calculated structure of biohybrid catalysts **Ru-X₂@NB4exp**. (a) Synthesis of **Ru-X₂** via salt-metathesis of maleimide-tagged GHII catalyst **Ru-Cl₂** and subsequent conjugation to NB4exp forming the artificial metalloenzymes **Ru-X₂@NB4exp**; Reaction conditions (I): 500 equiv. Acetone, 500 equiv. NaX, RT, 36 or 72 h; Reaction conditions (II): H₂O/DMSO (9:1), 10 mM Tris-HX (pH 7.4), 200 mM KX, 100 μ M Ru-X₂ (5 equiv.), 20 μ M NB4exp (1 equiv.), RT, 1 h. (b) Structure of **Ru-Cl₂@NB4exp**. (c) Structure of **Ru-Br₂@NB4exp**. (d) Structure of **Ru-I₂@NB4exp**. The structures were calculated based previously published structure of NB4exp [55] and visualized with YASARA software. See further images of the structures from different angles in Fig. S3 in the Supporting information.

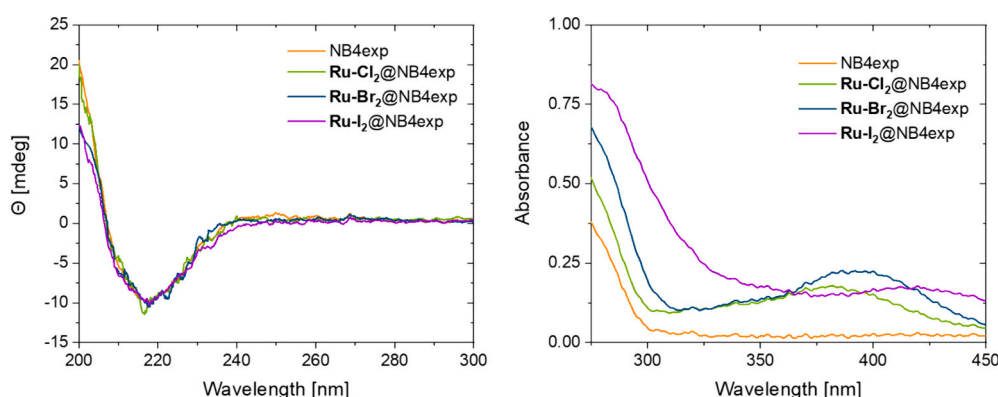


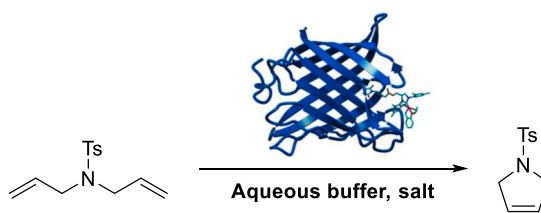
Fig. 3. Characterization of NB4exp (orange) and the conjugates **Ru-Cl₂@NB4exp** (green), **Ru-Br₂@NB4exp** (blue) and **Ru-I₂@NB4exp** (violet). (a) CD spectra in MES buffer (20 mM, pH 5.5). Potassium halide salts were not added due to the strong absorption in the region of the CD signal, spectra were recorded immediately after preparation of the biohybrid catalyst. (b) UV-vis spectra in MES buffer (20 mM, pH 5.5) containing potassium halide salt (250 mM). (For interpretation of the references to colour in this figure legend, the reader is referred to the web version of this article.)

X₂@NB4exp) for aqueous RCM of the benchmark substrate *N,N*-diallyltosylamide (Table 1). The robust protein scaffold tolerates water-miscible co-solvents, thus the use of 30% 1,4-dioxane ensuring solution homogeneity did not lead to protein denaturation. In these experiments, the effect of different aqueous buffer solutions and their interplay with the halide ligands on the catalytic performance of the biohybrid catalysts was evaluated. With **Ru-Cl₂@NB4exp**, TONs between 31 and 36 were observed in all buffers at pH 5.5 (Entries 1–3). The

use of acetate was leading to the lowest TONs. These TONs are in good agreement with our previous reports. [55] The decrease of the pH in acetate buffer to pH 4.0 led as expected to an improvement of the TON to 45 (Entry 4) which is in line with the general observation of aqueous olefin metathesis proceeding better under acidic conditions. [3,23] Comparably lower TONs of 19 to 27 were observed with **Ru-Br₂@NB4exp** under all investigated conditions (Entries 6–9). The substitution of chloride by iodide (**Ru-I₂@NB4exp**) gave the highest TONs

Table 1

Comparison of different buffers for the RCM *N,N*-diallyltosylamide catalyzed by biohybrid catalysts **Ru-X₂@NB4exp**.



Entry ^{a)}	Catalyst	Buffer	TON ^{b,c)}
1	Ru-Cl₂@NB4exp	Acetate (pH 5.5)	31
2		Phosphate (pH 5.5)	34
3		MES (pH 5.5)	36
4		Acetate (pH 4.0)	45
5		-	35
6	Ru-Br₂@NB4exp	Acetate (pH 5.5)	25
7		Phosphate (pH 5.5)	21
8		MES (pH 5.5)	19
9		Acetate (pH 4.0)	27
10		-	n.d.
11	Ru-I₂@NB4exp	Acetate (pH 5.5)	40
12		Phosphate (pH 5.5)	48
13		MES (pH 5.5)	53
14		Acetate (pH 4.0)	53
15		-	42

a) Reaction conditions: V = 0.5 mL, water/1,4-dioxane (7:3), 250 mM KX, 20 mM buffer (pH 5.5), 2.5 mM *N,N*-diallyltosylamide, 25 μ M **Ru-X₂@NB4exp** (1 mol%), 30 °C, 20 h reaction time. b) Determined by GC-MS analysis. c) Δ (TON) = \pm 3.

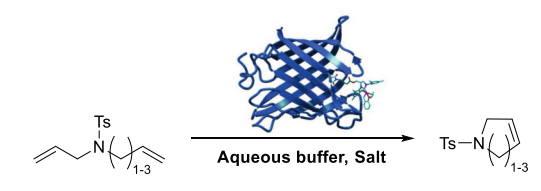
between 40 and 53 at pH 5.5 (Entries 11 to 13). The TON was improved up to 48% in comparison with the chloride complex in MES buffer (pH 5.5). For **Ru-I₂@NB4exp**, the use of acetate at pH 5.5 led to a decrease of the TON by 25%. When using salt-supplemented water at pH 7.0 (Entry 5), similar TONs as in the weakly coordinating buffers at pH 5.5 were observed with **Ru-Cl₂@NB4exp**. No catalysis was observed in pure potassium bromide solution at pH 7.0 with **Ru-Br₂@NB4exp**, probably due to lower protein/catalyst stability (Entry 10). In contrast, the TON of the reaction in pure water was lower when compared to the weakly coordinating buffers at pH 5.5 with **Ru-I₂@NB4exp** (Entry 15).

3.3. Ring-closing metathesis forming *N*-heterocycles with increased ring size

RCM reactions forming six- and seven-membered heterocycles with the halide-substituted biohybrid catalysts **Ru-X₂@NB4exp** were studied (Table 2). Each catalyst formed RCM products for all three substrates. Higher conversions were observed for the six-membered cycle (Entries 5–7) over the five-membered cycle with all catalysts (Entries 1–3). Especially for the known biohybrid catalyst **Ru-Cl₂@NB4exp**, a two-fold increase of the TON was observed. The increase for the dibromide analogue was only small. The highest TON of 74 was achieved using the diiodide homolog. With the increase of ring size to seven (Entries 9–11), the TON dropped for **Ru-Cl₂@NB4exp** to 23. In contrast, slightly higher TONs compared to the reactions forming smaller heterocycles were observed with the halide-substituted analogues **Ru-Br₂@NB4exp** and **Ru-I₂@NB4exp**. Non-productive side-reactions such as olefin isomerization proceeding via β -hydride elimination [50] were not observed for any catalyst-substrate combination.

Table 2

RCM for substrates leading to heterocycles with increased ring size catalyzed by the biohybrid catalysts **Ru-X₂@NB4exp**.



Entry ^{a)}	Substrate	Product	Catalyst	TON ^{b,c)}
1			Ru-Cl₂@NB4exp	36
2			Ru-Br₂@NB4exp	19
3			Ru-I₂@NB4exp	53
4			NB4exp	-
5			Ru-Cl₂@NB4exp	63
6			Ru-Br₂@NB4exp	25
7			Ru-I₂@NB4exp	74
8			NB4exp	-
9			Ru-Cl₂@NB4exp	23
10			Ru-Br₂@NB4exp	26
11			Ru-I₂@NB4exp	76
12			NB4exp	-

a) Reaction conditions: V = 0.5 mL, water/1,4-dioxane (7:3), 250 mM KX, 20 mM buffer (pH 5.5), 2.5 mM dialkenyltosylamide, 25 μ M **Ru-X₂@NB4exp** (1 mol%), 30 °C, 20 h reaction time. b) Determined by GC-MS analysis, c) Δ (TON) = \pm 3.

4. Discussion

Molecular modelling using YASARA software suggested that the halide substitution did not change the overall binding situation for all conjugates. In all conjugates, one halide ligand is directed towards the protein backbone and the other is directed towards the surface, thus being susceptible to the aqueous environment. Ligand exchange of chloride with water or hydroxide is assumed to be the most prominent decomposition pathway of GH-catalyst. [26] With our experimental setup, some insight into the effect of the halide ligand with the hydrophobic environment provided by the cavity of NB4exp was obtained. A general trend that the iodide based biohybrid catalyst give higher TONs compared to the chloride catalyst was observed, while the bromide based biohybrid catalysts gives lower TONs.

These experiments follow the rule that weakly coordinating buffers are more suitable compared to stronger coordinating buffers such as acetate which negatively influenced the TON of **Ru-Cl₂@NB4exp** and **Ru-I₂@NB4exp** at pH 5.5. [26,74] In acetate solution, the formation of acetate-chelated GH complexes is likely occurring. Stronger coordinating buffers are reported to decrease the efficiency of aqueous olefin metathesis. [24,26] In contrast, **Ru-Br₂@NB4exp**, exhibits the highest TONs in this buffer. The replacement with the typically unfavored acetate performing best with bromide underlines the unfavorable character of this ligand. Decreased stability of the intermediate species is also reported for other bromide-substituted ruthenium olefin metathesis catalysts. [75] In line with previous reports on aqueous olefin metathesis proceeding better under acidic conditions, a lower pH value of the acetate buffer increased the TONs for all biohybrid catalysts. [23]

The different behavior of the iodide substituted biohybrid catalysts can be explained by the hydrophobicity of the iodide ligand. In contrast to chloride, iodide is not able to form hydrogen bonds with the aqueous environment. [76] Together with the effects of the protein cavity, **Ru-I₂@NB4exp** is protected from decomposition/inactivation in the aqueous solution. These effects have also been reported in wet organic reaction media. [52,53] We propose that a higher hydrophobicity at the Ru-center stabilizes the complex in the presence of water. In aqueous

solution, this effect is less prominent than in organic media. Furthermore, the relative degree of improvement of catalyst performance by iodide ligands (1.5 fold) is lower compared to the biohybrid catalyst reported by Tanaka et al. (3 to 4 fold) [22] which is in agreement with the solvent susceptibility of the ruthenium center. The NB4exp scaffold is not capable of suppressing ligand exchange completely in the protein environment. Nevertheless, the hydrophobic cavity of NB4exp has a stabilizing effect on the ruthenium center reducing decomposition reactions. The expected catalyst dimerization assumed to be occurring under aqueous conditions [77] is sterically less favored due to the protein backbone. β -Hydride elimination typically occurs during the preparation of macrocycles, [50] but was not observed with the biohybrid catalysts. This enabled the successful formation of unsaturated six- and seven-membered *N*-heterocycles especially with $\text{Ru-I}_2\text{@NB4exp}$. To the best of our knowledge, these results represent the highest TONs reported for RCM yielding six- and seven-membered heterocycles with biohybrid catalysts exceeding the TONs reported by Tanaka et al. although under less favorable conditions. [20,22]

5. Conclusion

In this study, bromide- and iodide-substituted GHII catalysts were conjugated to the engineered β -barrel protein NB4exp. The bio-conjugates were characterized by ICP-OES, CD spectroscopy, UV-Vis spectroscopy and ESI MS. Both halide-substituted biohybrid catalysts promoted aqueous RCM of dialkenyltosylamides. While the dibromido homolog suffered from low stability leading to decreased TONs in RCM reactions under the conditions tested compared to the dichloride catalyst, the exchange with iodide ligands led to significant improvement of the TONs. The diiodide catalyst showed increased RCM activity for substrates forming six- and seven-membered heterocycles. None of the tested biohybrid catalysts promoted undesired side-reactions. Substitution of the chlorido ligands with iodide appears to be a promising approach to further tune aqueous olefin metathesis.

Author contributions

AI and DW conducted the experimental work. AI analyzed the data and wrote the manuscript. DW and JO reviewed the manuscript. US and JO managed the research.

Notes

The authors declare no competing financial interest.

CRedit authorship contribution statement

Aaron A. Ingram: Writing – original draft, Methodology, Investigation, Formal analysis. **Dong Wang:** Writing – review & editing, Validation, Methodology, Data curation. **Ulrich Schwaneberg:** Writing – review & editing, Project administration, Funding acquisition. **Jun Okuda:** Writing – review & editing, Writing – original draft, Supervision, Conceptualization.

Declaration of competing interest

The authors declare the following financial interests/personal relationships which may be considered as potential competing interests:

Jun Okuda reports financial support was provided by BMBF Bundesministerium für Bildung und Forschung. If there are other authors, they declare that they have no known competing financial interests or personal relationships that could have appeared to influence the work reported in this paper.

Data availability

Data will be made available on request.

Acknowledgement

We acknowledge the BioökonomieREVIER_INNO PlastiQuant (FKZ:031B0918E) and the German Federal Ministry of Education and Research (BMBF) for financial support. We would like to thank Dr. Daniel F. Sauer and Dr. Ulrich Markel for the helpful discussions.

Appendix A. Supplementary data

Supplementary data to this article can be found online at <https://doi.org/10.1016/j.jinorgbio.2024.112616>.

References

- [1] D. Bartscher, K. Grela, Aqueous olefin metathesis, *Angew. Chem. Int. Ed.* 48 (2009) 442–454, <https://doi.org/10.1002/anie.200801451>.
- [2] J. Tomasek, J. Schatz, Olefin metathesis in aqueous media, *Green Chem.* 15 (2013) 2317–2338, <https://doi.org/10.1039/c3gc41042k>.
- [3] V. Sabatino, T.R. Ward, Aqueous olefin metathesis: recent developments and applications, *Beilstein J. Org. Chem.* 15 (2019) 445–468, <https://doi.org/10.3762/bjoc.15.39>.
- [4] T. Matsuo, Functionalization of ruthenium olefin-metathesis catalysts for interdisciplinary studies in chemistry and biology, *Catalysts* 11 (2021) 359, <https://doi.org/10.3390/catal11030359>.
- [5] G.C. Fu, S.T. Nguyen, R.H. Grubbs, Catalytic ring-closing metathesis of functionalized dienes by a ruthenium Carbene complex, *J. Am. Chem. Soc.* 115 (1993) 9856–9857, <https://doi.org/10.1021/ja00074a085>.
- [6] E.-J.Y. Boisvert, H.C. Max, D.E. Fogg, Rapid aerial oxidation of ruthenium-Dithiocatcholate catalysts: a challenge to Stereoretentive olefin metathesis, *ACS Catal.* 13 (2023) 2885–2891, <https://doi.org/10.1021/acscatal.2c06168>.
- [7] S. Wu, Y. Zhou, D. Gerngross, M. Jeschek, T.R. Ward, Chemo-enzymatic cascades to produce cycloalkenes from bio-based resources, *Nat. Commun.* 10 (2019) 5060, <https://doi.org/10.1038/s41467-019-13071-y>.
- [8] T. Tiso, D.F. Sauer, K. Beckerle, C.C. Blesken, J. Okuda, L.M. Blank, A combined bio-chemical synthesis route for 1-Octene sheds light on Rhamnolipid structure, *Catalysts* 10 (2020) 874, <https://doi.org/10.3390/catal10080874>.
- [9] V. Sabatino, J.G. Rebelein, T.R. Ward, “close-to-release”: spontaneous bioorthogonal uncaging resulting from ring-closing metathesis, *J. Am. Chem. Soc.* 141 (2019) 17048–17052, <https://doi.org/10.1021/jacs.9b07193>.
- [10] D.F. Sauer, Y. Qu, M.A.S. Mertens, J. Schiffels, T. Polen, U. Schwaneberg, J. Okuda, Biohybrid catalysts for sequential one-pot reactions based on an engineered transmembrane protein, *Catal. Sci. Technol.* 9 (2019) 942–946, <https://doi.org/10.1039/c8cy02236d>.
- [11] M.A.S. Mertens, D.F. Sauer, U. Markel, J. Schiffels, J. Okuda, U. Schwaneberg, Chemoenzymatic cascade for stilbene production from cinnamic acid catalyzed by ferulic acid decarboxylase and an artificial metatasease, *Catal. Sci. Technol.* 9 (2019) 5572–5576, <https://doi.org/10.1039/c9cy01412h>.
- [12] Y.A. Lin, J.M. Chalker, B.G. Davis, Olefin metathesis for site-selective protein modification, *ChemBioChem* 10 (2009) 959–969, <https://doi.org/10.1002/cbic.200900002>.
- [13] Y.A. Lin, J.M. Chalker, N. Floyd, G.J.L. Bernardes, B.G. Davis, Allyl sulfides are privileged substrates in aqueous cross-metathesis: application to site-selective protein modification, *J. Am. Chem. Soc.* 130 (2008) 9642–9643, <https://doi.org/10.1021/ja8026168>.
- [14] B. Bhushan, Y.A. Lin, M. Bak, A. Phanumartwiwath, N. Yang, M.K. Bilyard, T. Tanaka, K.L. Hudson, L. Lercher, M. Stegmann, S. Mohammed, B.G. Davis, Genetic incorporation of olefin cross-metathesis reaction tags for protein modification, *J. Am. Chem. Soc.* 140 (2018) 14599–14603, <https://doi.org/10.1021/jacs.8b09433>.
- [15] X. Lu, L. Fan, C.B. Phelps, C.P. Davie, C.P. Donahue, Ruthenium promoted on-DNA ring-closing metathesis and cross-metathesis, *Bioconjug. Chem.* 28 (2017) 1625–1629, <https://doi.org/10.1021/acs.bioconjchem.7b00292>.
- [16] S.N.W. Toussaint, R.T. Calkins, S. Lee, B.W. Michel, Olefin metathesis-based fluorescent probes for the selective detection of ethylene in live cells, *J. Am. Chem. Soc.* 140 (2018) 13151–13155, <https://doi.org/10.1021/jacs.8b05191>.
- [17] K. Vong, S. Eda, Y. Kadota, I. Nasibullin, T. Wakatake, S. Yokoshima, K. Shirasu, K. Tanaka, An artificial metalloenzyme biosensor can detect ethylene gas in fruits and Arabidopsis leaves, *Nat. Commun.* 10 (2019) 5746, <https://doi.org/10.1038/s41467-019-13758-2>.
- [18] N.S. Schunck, S. Mecking, In vivo olefin metathesis in microalgae upgrades lipids to building blocks for polymers and chemicals, *Angew. Chem. Int. Ed.* 61 (2022) e202211285, <https://doi.org/10.1002/anie.202211285>.
- [19] M. Jeschek, R. Reuter, T. Heinisch, C. Trindler, J. Klehr, S. Panke, T.R. Ward, Directed evolution of artificial metalloenzymes for in vivo metathesis, *Nature* 537 (2016) 661–665, <https://doi.org/10.1038/nature19114>.
- [20] S. Eda, I. Nasibullin, K. Vong, N. Kudo, M. Yoshida, A. Kurbangalieva, K. Tanaka, Biocompatibility and therapeutic potential of glycosylated albumin artificial

- metalloenzymes, *Nature Catal.* 2 (2019) 780–792, <https://doi.org/10.1038/s41929-019-0317-4>.
- [21] I. Nasibullin, I. Smirnov, P. Ahmadi, K. Vong, A. Kurbangalieva, K. Tanaka, Synthetic prodrug design enables biocatalytic activation in mice to elicit tumor growth suppression, *Nat. Commun.* 13 (2022) 39, <https://doi.org/10.1038/s41467-021-27804-5>.
- [22] I. Nasibullin, H. Yoshioka, A. Mukaimine, A. Nakamura, Y. Kusakari, T.C. Chang, K. Tanaka, Catalytic olefin metathesis in blood, *Chem. Sci.* 14 (2023) 11033–11039, <https://doi.org/10.1039/d3sc03785a>.
- [23] M.A. Dunbar, S.L. Balof, A.N. Roberts, E.J. Valente, H.-J. Schanz, pH-responsive ruthenium-based olefin metathesis catalysts: controlled ring-opening metathesis polymerization in alcoholic and aqueous media upon acid addition, *Organometallics* 30 (2010) 199–203, <https://doi.org/10.1021/om100633f>.
- [24] D.C. Church, L. Takiguchi, J.K. Pokorski, Optimization of ring-opening metathesis polymerization (ROMP) under physiologically relevant conditions, *Polym. Chem.* 11 (2020) 4492–4499, <https://doi.org/10.1039/d0py00716a>.
- [25] A.Y. Goudreault, D.M. Walden, D.L. Nascimento, A.G. Botti, S.N. Steinmann, C. Michel, D.E. Fogg, Hydroxide-induced degradation of olefin metathesis catalysts: a challenge for metathesis in alkaline media, *ACS Catal.* 10 (2020) 3838–3843, <https://doi.org/10.1021/acscatal.9b05163>.
- [26] T. Matsuo, T. Yoshida, A. Fujii, K. Kawahara, S. Hirota, Effect of Added Salt on Ring-Closing Metathesis Catalyzed by a Water-Soluble Hoveyda–Grubbs Type Complex To Form N-Containing Heterocycles in Aqueous Media, *Organometallics* 32 (2013) 5313–5319, <https://doi.org/10.1021/om4005302>.
- [27] C.C. James, P.C.M. Laan, B. de Bruin, J.N.H. Reek, Kinetic protection of a water-soluble olefin metathesis catalyst for potential use under biological conditions, *ChemCatChem* (2023), <https://doi.org/10.1002/cctc.202201272>.
- [28] C. Lo, M.R. Ringenberg, D. Gnanth, Y. Wilson, T.R. Ward, Artificial metalloenzymes for olefin metathesis based on the biotin-(strept)avidin technology, *Chem. Commun.* 47 (2011) 12065–12067, <https://doi.org/10.1039/c1cc15004a>.
- [29] C. Mayer, D.G. Gillingham, T.R. Ward, D. Hilvert, An artificial metalloenzyme for olefin metathesis, *Chem. Commun.* 47 (2011) 12068–12070, <https://doi.org/10.1039/c1cc15005g>.
- [30] T. Matsuo, C. Imai, T. Yoshida, T. Saito, T. Hayashi, S. Hirota, Creation of an artificial metalloprotein with a Hoveyda–Grubbs catalyst moiety through the intrinsic inhibition mechanism of alpha-chymotrypsin, *Chem. Commun.* 48 (2012) 1662–1664, <https://doi.org/10.1039/c2cc16898g>.
- [31] M. Basauri-Molina, D.G.A. Verhoeven, A.J. van Schaik, H. Kleijn, R.J.M. Klein Gebbink, Ring-closing and cross-metathesis with artificial Metalloenzymes created by covalent active site-directed hybridization of a lipase, *Chemistry* 21 (2015) 15676–15685, <https://doi.org/10.1002/chem.201502381>.
- [32] J. Zhao, A. Kajetanowicz, T.R. Ward, Carbonic anhydrase II as host protein for the creation of a biocompatible artificial metathetase, *Org. Biomol. Chem.* 13 (2015) 5652–5655, <https://doi.org/10.1039/c5ob00428d>.
- [33] S. Fischer, T.R. Ward, A.D. Liang, Engineering a metathesis-catalyzing artificial Metalloenzyme based on HaloTag, *ACS Catal.* 11 (2021) 6343–6347, <https://doi.org/10.1021/acscatal.1c01470>.
- [34] F. Philippart, M. Airlt, S. Gotzen, S.J. Tenne, M. Bocola, H.H. Chen, L. Zhu, U. Schwaneberg, J. Okuda, A hybrid ring-opening metathesis polymerization catalyst based on an engineered variant of the beta-barrel protein FluA, *Chemistry* 19 (2013) 13865–13871, <https://doi.org/10.1002/chem.201301515>.
- [35] D.F. Sauer, M. Bocola, C. Broglia, M. Airlt, L.L. Zhu, M. Brocker, U. Schwaneberg, J. Okuda, Hybrid ruthenium ROMP catalysts based on an engineered variant of beta-barrel protein FluA DeltaCVF(tev): effect of spacer length, *Chem. Asian J.* 10 (2015) 177–182, <https://doi.org/10.1002/asia.201403005>.
- [36] M.T. Reetz, Directed evolution of artificial Metalloenzymes: a universal means to tune the selectivity of transition metal catalysts? *Acc. Chem. Res.* 52 (2019) 336–344, <https://doi.org/10.1021/acs.accounts.8b00582>.
- [37] M. Durrenberger, T.R. Ward, Recent achievements in the design and engineering of artificial metalloenzymes, *Curr. Opin. Chem. Biol.* 19 (2014) 99–106, <https://doi.org/10.1016/j.cbpa.2014.01.018>.
- [38] M.S. Sanford, J.A. Love, R.H. Grubbs, Mechanism and activity of ruthenium olefin metathesis catalysts, *J. Am. Chem. Soc.* 123 (2001) 6543–6554, <https://doi.org/10.1021/ja010624k>.
- [39] J. Wappel, C.A. Urbina-Blanco, M. Abbas, J.H. Albering, R. Saf, S.P. Nolan, C. Slugovc, Halide exchanged Hoveyda-type complexes in olefin metathesis, *Beilstein J. Org. Chem.* 6 (2010) 1091–1098, <https://doi.org/10.3762/bjoc.6.125>.
- [40] R. Gawin, K. Grela, Synthesis of stable ruthenium olefin metathesis catalysts with mixed anionic ligands, *Eur. J. Inorg. Chem.* 2012 (2012) 1477–1484, <https://doi.org/10.1002/ejic.201101048>.
- [41] J. Hartung, P.K. Dornan, R.H. Grubbs, Enantioselective olefin metathesis with cyclometalated ruthenium complexes, *J. Am. Chem. Soc.* 136 (2014) 13029–13037, <https://doi.org/10.1021/ja506611k>.
- [42] T.J. Seiders, D.W. Ward, R.H. Grubbs, Enantioselective ruthenium-catalyzed ring-closing metathesis, *Org. Lett.* 3 (2001) 3225–3228, <https://doi.org/10.1021/ol0165692>.
- [43] T.W. Funk, J.M. Berlin, R.H. Grubbs, Highly active chiral ruthenium catalysts for asymmetric ring-closing olefin metathesis, *J. Am. Chem. Soc.* 128 (2006) 1840–1846, <https://doi.org/10.1021/ja055994d>.
- [44] V. Paradiso, F. Bertolasi, F. Grisi, Novel olefin metathesis ruthenium catalysts bearing backbone-substituted unsymmetrical NHC ligands, *Organometallics* 33 (2014) 5932–5935, <https://doi.org/10.1021/om500731k>.
- [45] V. Paradiso, F. Bertolasi, C. Costabile, F. Grisi, Ruthenium olefin metathesis catalysts featuring unsymmetrical N-heterocyclic carbenes, *Dalton Trans.* 45 (2016) 561–571, <https://doi.org/10.1039/c5dt03758a>.
- [46] N.B. Nechmad, V. Kobernik, N. Tarannam, R. Phatake, O. Eivgi, S. Kozuch, N. G. Lemcoff, Reactivity and selectivity in ruthenium sulfur-chelated Diiodo catalysts, *Angew. Chem. Int. Ed.* 60 (2021) 6372–6376, <https://doi.org/10.1002/anie.202014929>.
- [47] R.S. Phatake, N.B. Nechmad, O. Reany, N.G. Lemcoff, Highly substrate-selective macrocyclic ring closing metathesis, *Adv. Synth. Catal.* 364 (2022) 1465–1472, <https://doi.org/10.1002/adsc.202101515>.
- [48] N.B. Nechmad, K. Iudanov, N. Tarannam, V. Kobernik, S. Kozuch, N.G. Lemcoff, Coordinating additives as activity modulators in Diiodo latent olefin metathesis catalysts, *ChemCatChem* 15 (2023) e202201690, <https://doi.org/10.1002/cctc.202201690>.
- [49] C.O. Blanco, D.L. Nascimento, D.E. Fogg, Routes to high-performing ruthenium-iodide catalysts for olefin metathesis: ligand lability is key to efficient halide exchange, *Organometallics* 40 (2021) 1811–1816, <https://doi.org/10.1021/acs.organomet.1c00253>.
- [50] A. Tracz, M. Matczak, K. Urbaniak, K. Skowerski, Nitro-Grela-type complexes containing iodides - robust and selective catalysts for olefin metathesis under challenging conditions, *Beilstein J. Org. Chem.* 11 (2015) 1823–1832, <https://doi.org/10.3762/bjoc.11.198>.
- [51] P.S. Engl, A. Tsygankov, J. De Jesus Silva, J.P. Lange, C. Copéret, A. Togni, A. Fedorov, Acrylate esters by Ethenolysis of maleate esters with Ru metathesis catalysts: an HTE and a Technoeconomic study, *Helv. Chim. Acta* 103 (2020), <https://doi.org/10.1002/hlca.202000035>.
- [52] C.O. Blanco, J. Sims, D.L. Nascimento, A.Y. Goudreault, S.N. Steinmann, C. Michel, D.E. Fogg, The impact of water on Ru-catalyzed olefin metathesis: potent deactivating effects even at low water concentrations, *ACS Catal.* 11 (2021) 893–899, <https://doi.org/10.1021/acscatal.0c04279>.
- [53] C.O. Blanco, D.E. Fogg, Water-accelerated decomposition of olefin metathesis catalysts, *ACS Catal.* 13 (2023) 1097–1102, <https://doi.org/10.1021/acscatal.2c05573>.
- [54] A.A. Ingram, K. Oike, Artificial biocatalysis: quo Vadis? *ChemCatChem* e202301759 (2024) <https://doi.org/10.1002/cctc.202301759>.
- [55] A.R. Grimm, D.F. Sauer, M.D. Davari, L. Zhu, M. Bocola, S. Kato, A. Onoda, T. Hayashi, J. Okuda, U. Schwaneberg, Cavity size engineering of a β -barrel protein generates efficient biohybrid catalysts for olefin metathesis, *ACS Catal.* 8 (2018) 3358–3364, <https://doi.org/10.1021/acscatal.7b03652>.
- [56] D.F. Sauer, T. Himiyama, K. Tachikawa, K. Fukumoto, A. Onoda, E. Mizohata, T. Inoue, M. Bocola, U. Schwaneberg, T. Hayashi, J. Okuda, A highly active biohybrid catalyst for olefin metathesis in water: impact of a hydrophobic cavity in a β -barrel protein, *ACS Catal.* 5 (2015) 7519–7522, <https://doi.org/10.1021/acscatal.5b01792>.
- [57] A. Onoda, K. Fukumoto, M. Airlt, M. Bocola, U. Schwaneberg, T. Hayashi, A rhodium complex-linked beta-barrel protein as a hybrid biocatalyst for phenylacetylene polymerization, *Chem. Commun.* 48 (2012) 9756–9758, <https://doi.org/10.1039/c2cc35165j>.
- [58] K. Fukumoto, A. Onoda, E. Mizohata, M. Bocola, T. Inoue, U. Schwaneberg, T. Hayashi, Rhodium-complex-linked hybrid biocatalyst: stereo-controlled Phenylacetylene polymerization within an engineered protein cavity, *ChemCatChem* 6 (2014) 1229–1235, <https://doi.org/10.1002/cctc.201301055>.
- [59] S. Kato, A. Onoda, A.R. Grimm, U. Schwaneberg, T. Hayashi, Construction of a whole-cell biohybrid catalyst using a $\text{Cp}^*\text{Rh(III)}$ -dithiophosphate complex as a precursor of a metal cofactor, *J. Inorg. Biochem.* 216 (2021) 111352, <https://doi.org/10.1016/j.jinorgbio.2020.111352>.
- [60] S. Kato, A. Onoda, A.R. Grimm, K. Tachikawa, U. Schwaneberg, T. Hayashi, Incorporation of a $\text{Cp}^*\text{Rh(III)}$ -dithiophosphate cofactor with latent activity into a protein scaffold generates a biohybrid catalyst promoting $\text{C(sp}^2\text{)}\text{-H}$ bond functionalization, *Inorg. Chem.* 59 (2020) 14457–14463, <https://doi.org/10.1021/acs.inorgchem.0c02245>.
- [61] S. Kato, A. Onoda, U. Schwaneberg, T. Hayashi, Evolutionary engineering of a $\text{Cp}^*\text{Rh(III)}$ complex-linked artificial Metalloenzyme with a chimeric beta-barrel protein scaffold, *J. Am. Chem. Soc.* 145 (2023) 8285–8290, <https://doi.org/10.1021/jacs.3c00581>.
- [62] S. Kato, A. Onoda, N. Taniguchi, U. Schwaneberg, T. Hayashi, Directed evolution of a $\text{Cp}^*\text{Rh(III)}$ -linked biohybrid catalyst based on a screening platform with affinity purification, *ChemBioChem* 22 (2021) 679–685, <https://doi.org/10.1002/cbic.202000681>.
- [63] T. Himiyama, D.F. Sauer, A. Onoda, T.P. Spaniol, J. Okuda, T. Hayashi, Construction of a hybrid biocatalyst containing a covalently-linked terpyridine metal complex within a cavity of aponitrobindin, *J. Inorg. Biochem.* 158 (2016) 55–61, <https://doi.org/10.1016/j.jinorgbio.2015.12.026>.
- [64] T. Himiyama, N. Taniguchi, S. Kato, A. Onoda, T. Hayashi, A pyrene-linked cavity within a beta-barrel protein promotes an asymmetric Diels–Alder reaction, *Angew. Chem. Int. Ed.* 56 (2017) 13618–13622, <https://doi.org/10.1002/anie.201704524>.
- [65] U. Markel, D.F. Sauer, M. Wittwer, J. Schifffels, H. Cui, M.D. Davari, K.W. Kröckert, S. Herres-Pawlis, J. Okuda, U. Schwaneberg, Chemogenetic evolution of a peroxidase-like artificial Metalloenzyme, *ACS Catal.* 11 (2021) 5079–5087, <https://doi.org/10.1021/acscatal.1c00134>.
- [66] D.F. Sauer, M. Wittwer, U. Markel, A. Minges, M. Spiertz, J. Schifffels, M.D. Davari, G. Groth, J. Okuda, U. Schwaneberg, Chemogenetic engineering of nitrobindin toward an artificial epoxidegenase, *Catal. Sci. Technol.* 11 (2021) 4491–4499, <https://doi.org/10.1039/d1cy00609f>.
- [67] D. Wang, A.A. Ingram, A. Okumura, T.P. Spaniol, U. Schwaneberg, J. Okuda, Benzyl C(sp³)-H bond oxidation with ketone selectivity by a cobalt(IV)-Oxo embedded in a beta-barrel protein, *Chemistry* 30 (2024) e202303066, <https://doi.org/10.1002/chem.202303066>.

- [68] H.E. Gottlieb, V. Kotlyar, A. Nudelman, NMR chemical shifts of common laboratory solvents as trace impurities, *J. Organomet. Chem.* 62 (1997) 7512–7515, <https://doi.org/10.1021/jo971176v>.
- [69] E. Krieger, G. Vriend, YASARA view - molecular graphics for all devices - from smartphones to workstations, *Bioinformatics* 30 (2014) 2981–2982, <https://doi.org/10.1093/bioinformatics/btu426>.
- [70] Y. Duan, C. Wu, S. Chowdhury, M.C. Lee, G. Xiong, W. Zhang, R. Yang, P. Cieplak, R. Luo, T. Lee, J. Caldwell, J. Wang, P. Kollman, A point-charge force field for molecular mechanics simulations of proteins based on condensed-phase quantum mechanical calculations, *J. Comput. Chem.* 24 (2003) 1999–2012, <https://doi.org/10.1002/jcc.10349>.
- [71] J. Wang, R.M. Wolf, J.W. Caldwell, P.A. Kollman, D.A. Case, Development and testing of a general amber force field, *J. Comput. Chem.* 25 (2004) 1157–1174, <https://doi.org/10.1002/jcc.20035>.
- [72] A. Jakalian, D.B. Jack, C.I. Bayly, Fast, efficient generation of high-quality atomic charges. AM1-BCC model: II. Parameterization and validation, *J. Comput. Chem.* 23 (2002) 1623–1641, <https://doi.org/10.1002/jcc.10128>.
- [73] M.F. Sanner, A.J. Olson, J.-C. Spehner, Reduced surface: an efficient way to compute molecular surfaces, *Biopolymers* 38 (1996) 305–320, [https://doi.org/10.1002/\(SICI\)1097-0282\(199603\)38:3%3C305::AID-BIP4%3E3.0.CO;2-Y](https://doi.org/10.1002/(SICI)1097-0282(199603)38:3%3C305::AID-BIP4%3E3.0.CO;2-Y).
- [74] J.C. Foster, M.C. Grocott, L.A. Arkinstall, S. Varlas, M.J. Redding, S.M. Grayson, R. K. O'Reilly, It is better with salt: aqueous ring-opening metathesis polymerization at neutral pH, *J. Am. Chem. Soc.* 142 (2020) 13878–13885, <https://doi.org/10.1021/jacs.0c05499>.
- [75] S.H. Hong, A.G. Wenzel, T.T. Salguero, M.W. Day, R.H. Grubbs, Decomposition of ruthenium olefin metathesis catalysts, *J. Am. Chem. Soc.* 129 (2007) 7961–7968, <https://doi.org/10.1021/ja0713577>.
- [76] G.A. Jeffrey, W. Saenger, *Hydrogen Bonding in Biological Structures*, Springer, Berlin, Heidelberg, 1991, pp. 161–163, <https://doi.org/10.1007/978-3-642-85135-3>.
- [77] D.L. Nascimento, M. Foscatto, G. Occhipinti, V.R. Jensen, D.E. Fogg, Bimolecular coupling in olefin metathesis: correlating structure and decomposition for leading and emerging ruthenium-Carbene catalysts, *J. Am. Chem. Soc.* 143 (2021) 11072–11079, <https://doi.org/10.1021/jacs.1c04424>.